

Distill3R: A Pipeline for Democratizing 3D Foundation Models on Commodity Hardware

Brandon Leblanc

*Immersive and Creative Technologies Lab
Concordia University
Montreal, Canada*

brandon.leblanc@mail.concordia.ca

Charalambos Poullis

*Immersive and Creative Technologies Lab
Concordia University
Montreal, Canada*

charalambos.poullis@concordia.ca

Abstract—While multi-view 3D reconstruction has shifted toward large-scale foundation models capable of inferring globally consistent geometry, their reliance on massive computational clusters for training has created a significant barrier to entry for most academic laboratories. To bridge this compute divide, we introduce Distill3R, a framework designed to distill the geometric reasoning of 3D foundation models into compact students fully trainable on a single workstation. Our methodology centers on two primary innovations: (1) an offline caching pipeline that decouples heavy teacher inference from the training loop through compressed supervision signals, and (2) a confidence-aware distillation loss that leverages teacher uncertainty to enable training on commodity hardware. We propose a 72M-parameter student model which achieves a 9x reduction in parameters and a 5x inference speedup compared to its 650M-parameter teacher. The student is fully trainable in under 3 days on a single workstation, whereas its teacher requires massive GPU clusters for up to a week. We demonstrate that the student preserves the structural consistency and qualitative geometric understanding required for functional 3D awareness. By providing a reproducible, single-workstation training recipe, Distill3R serves as an exploratory entry point for democratized 3D vision research and efficient edge deployment. This work is not intended to compete with state-of-the-art foundation models, but to provide an accessible research baseline for laboratories without access to large-scale compute to train and specialize models on their own domain-specific data at minimal cost.

Source code available at

<https://github.com/TheFourthKaramazov/Distill3R>

Index Terms—Knowledge Distillation, 3D Reconstruction, Efficient AI, Democratizing AI.

I. INTRODUCTION

Unconstrained multi-view reconstruction methods that directly predict 3D geometry in a single forward pass have advanced rapidly since the introduction of DUS3R [1]. By demonstrating that a neural network could infer consistent geometry and implicit relative camera poses from image pairs without following the classical pipeline of Structure-from-Motion (SfM) and Multi-View Stereo (MVS) [2]–[8], DUS3R marked a turning point in learned 3D reconstruction. Its pairwise reconstruction and subsequent procedural global alignment strategy have been surpassed by fully end-to-end architectures capable of processing all views jointly

The Natural Sciences and Engineering Research Council of Canada (NSERC) supported this work through the CGS-M scholarship.

and producing globally consistent reconstructions in a single step [9]–[11], [11]–[15]. Using global attention mechanisms and large-scale training, these models follow a familiar trajectory in deep learning: rapid gains driven by exponential increases in both model capacity and dataset scale [16]–[24]. For example, Fast3R [9] is trained on 128 A100 GPUs for 6.13 days and VGGT [10] on 64 A100 GPUs for 9 days, containing approximately 650 M and 1 B parameters, respectively. Although these advances have shown impressive results, they have also concentrated progress within a small number of frontier labs equipped with vast computational resources, thereby preventing most labs from building upon and improving these models, which results in a bottleneck for research progress in this domain. Moreover, their size and inference cost make them impractical for deployment on edge devices, where 3D reconstruction is most valuable, such as in robotics, medical applications, and autonomous navigation [25]–[30].

This disparity between high-capacity research models and real-world deployment environments has created a divergence between innovation and accessibility. While breakthroughs in multi-view geometry increasingly rely on massive computation, many research and industry groups lack the resources to train or deploy such systems. This is evidenced by recent work surrounding VGGT being training-free [30]–[33], demonstrating an inherent bias towards improving efficiency and performance while avoiding training. As a result, the community faces a structural bottleneck: the pursuit of absolute performance has outpaced our collective ability to participate in the development and iteration of these models, gate-keeping research innovation. Addressing this requires a paradigm shift that prioritizes the establishment of accessible research pipelines over marginal gains in accuracy. Rather than attempting to replicate the industrial-scale infrastructure of frontier labs, the primary contribution of this work is to provide a high-efficiency methodology that lowers the barrier to entry. By establishing a reproducible framework for distillation, we enable the broader community to leverage high-capacity models by proxy and explore new research directions in 3D vision using commodity hardware.

To this end, we introduce Distill3R, a novel distillation framework [25], [34]–[36] designed to address this accessi-

bility problem in 3D vision. Distill3R enables researchers and practitioners to train compact, high-performance reconstruction models on a single workstation, achieving up to a $9\times$ reduction in model size relative to the teacher. We adopt Fast3R [9] as the teacher due to its balance of efficiency and accuracy. Inspired by TinyViT [25], Distill3R introduces an offline cache mechanism that stores teacher-generated supervision signals, eliminating the need for expensive online teacher inference during training. By transforming foundation model distillation into a task feasible on commodity hardware, this approach enables scalable experimentation and rapid iteration without the need for multi-million dollar infrastructure.

Through our evaluation, we show that a 72 M-parameter student trained via Distill3R serves as a functional, exploratory entry point for resource-constrained 3D vision research. While absolute precision on benchmarks like 7-Scenes exhibits a quantitative drop compared to the teacher, we demonstrate that the student successfully preserves the structural and topological consistency required for general spatial awareness and monocular 3D reconstruction as well as a significantly superior adherence to absolute metric scale across both indoor and extreme out-of-distribution (OOD) object-centric scenes. This consistency is crucial for downstream robotics tasks such as reactive obstacle avoidance and local occupancy mapping [37], where high update rates and qualitative scene understanding often outweigh millimetric precision [38]–[40]. We identify that the observed quantitative gap is primarily driven by subtle geometric warping and scale ambiguities that impact regression metrics but do not preclude functional utility. Despite these trade-offs, our confidence-aware distillation loss successfully stabilizes training on commodity hardware, yielding a student with a $5\times$ inference speedup. By shifting the focus from inference-only deployment to an accessible training pipeline, we empower the community to modify and refine these models without requiring industrial-scale infrastructure.

Our main technical contributions are as follows:

1. Distill3R, a novel distillation framework for learned 3D reconstruction that employs an offline cache mechanism to enable training on a single workstation.
2. A confidence-aware distillation loss, which leverages cached teacher confidence values for both direct supervision and geometric loss weighting, improving training stability by taking advantage of learned teacher confidence values for geometric weighting rather than degenerate student predictions.
3. Democratized research baseline: We provide a comprehensive characterization of the trade-offs between model size and reconstruction fidelity, offering a $9\times$ parameter reduction and $5\times$ inference speedup as an exploratory roadmap for accessible 3D vision research.

II. RELATED WORK

A. Procedural and differentiable pipelines

The traditional Structure-from-Motion (SfM) pipeline [4], [7], [41], composed of sequential steps that include feature extraction [42]–[46], feature matching [47]–[50], correspondence search, sparse reconstruction, and multi-view stereo (MVS)

[51]–[53], remains the most accessible and interpretable approach to recover 3D geometry from unordered images when hardware resources are limited. However, each stage of this pipeline introduces cumulative error and often fails under real-world conditions such as textureless regions, limited overlap, or dynamic scenes. Furthermore, the entire process can take hours as the number of input images increases [4], [54]. Although recent work has integrated learning-based improvements such as robust correspondence search [47], [55], learned features [56], [57], and differentiable bundle adjustment [3], [58]–[60], the pipeline remains slow, fragile, and cumbersome to deploy outside controlled datasets.

B. Geometric foundation models

To address the limitations of procedural pipelines, the field turned toward single pass, feed-forward networks. DUS3R pioneered this direction by regressing dense point maps from image pairs. The two important contributions that make this possible are carefully curated datasets [27], [29], [61]–[67] and the point map representation [1]. Rather than solving for camera intrinsics and extrinsics explicitly to triangulate points [41], DUS3R and subsequent models [9]–[11], [13], [24], [68]–[70] train a model to directly regress a dense 2D coordinate map with the same dimensions as the input images, creating a one-to-one mapping between image pixels and 3D coordinates. This representation unifies geometry and pose while allowing geometric priors to be learned through the mapping from pixel to 3D point. These models also predict a pixel-wise confidence map with the same dimensions as the input image and the output point map, allowing the system to learn its own uncertainty and filter out unreliable predictions. This dense and confidence-aware regression serves as the foundation of our objective function in the distillation framework. However, these methods [1], [11], [15] are fundamentally pairwise; achieving global consistency across a scene requires costly post-hoc global alignment solvers such as PnP [71]–[73] that scale poorly. Sequential approaches like [13], [70] attempt to mitigate this via memory mechanisms but suffer from drift accumulation over long sequences. Most recently, global foundation models like Fast3R [9], VGGT [10], and π^3 [24] have achieved state-of-the-art results by processing all views simultaneously using global attention mechanisms. Although these models solve the global consistency problem in a single forward pass, they do so at a significant computational cost. With parameters ranging from 650 M to more than 1 B and training requirements exceeding 100 A100 GPUs, these heavyweight models remain inaccessible for research iteration and deployment on edge devices, reinforcing the infrastructure bottleneck that prevents the broader community from participating in the development of 3D vision foundation models.

C. Efficient 3D vision and distillation

Knowledge Distillation (KD) [34]–[36] is a standard technique for model compression, yet its application to generalizable 3D reconstruction remains underexplored. Distilled

encoders such as DUNE [74], which we use in our student model, have managed to surpass their teachers' performance in 3D tasks by using heterogeneous co-distillation to achieve knowledge synthesis and refinement while significantly reducing parameter count. Previous efforts in 3D-aware KD have largely focused on disparate tasks, such as compressing NeRFs [75], [76] or depth estimation [77]–[79]. In the multi-view domain, KD-MVS [80] applies distillation to improve depth accuracy without ground-truth labels, but it does not prioritize model compression or reducing heavy memory requirements and relies on the restrictive assumption of known camera parameters. Close to our work, [81] distills DUST3R but remains limited to per-scene optimization which is of limited use. They do not attempt to distill a general-purpose model. Concurrently, inference-only acceleration methods have emerged: QuantVGGT [33] applies post-training quantization to compress VGGT to 4 bits; AVGGT [30] uses mechanistic interpretability insights [82] to remove global attention in early decoder layers where correspondences are not optimized; Faster VGGT [31] uses block sparse attention to increase efficiency; while FastVGGT [32] utilizes token pruning to speed up inference. Although effective for deployment, these are strictly inference-time optimizations that do not address the high computational requirements of training. This creates a documented bias in current research toward improving performance while avoiding the training process due to prohibitive infrastructure costs.

III. METHOD

A. Problem Definition

We address the task of unconstrained multi-view 3D reconstruction. Given a set of N unposed 2D images $\mathcal{I} = \{I_1, \dots, I_N\}$ depicting a scene, the goal is to infer the 3D geometry of the scene. Let T be a pre-trained teacher model and S be our compact student model. For any given image $I_k \in \mathcal{I}$, both models are trained to predict dense 2D maps that encode 3D information at a resolution $H \times W$. The specific outputs we aim to distill from the teacher T are:

- Global 3D point map: $\mathbf{P}_k^g \in \mathbb{R}^{H \times W \times 3}$. For each pixel (i, j) in image I_k , this map stores the predicted 3D coordinate $\mathbf{p}_{k,ij}^g$ in a single, consistent global reference frame for the entire scene.
- Local 3D point map: $\mathbf{P}_k^\ell \in \mathbb{R}^{H \times W \times 3}$. For each pixel (i, j) , this map stores the 3D coordinate $\mathbf{p}_{k,ij}^\ell$ relative to its own local camera frame.
- Confidence maps: $C_k^g, C_k^\ell \in \mathbb{R}^{H \times W}$. These maps store the teacher's per-pixel confidence $c_{k,ij} \in [0, \infty)$ in the accuracy of its corresponding global and local 3D predictions.

Our objective is to train the student model S such that its predicted outputs, denoted $(\mathbf{P}^{s,g}, \mathbf{P}^{s,\ell}, C^{s,g}, C^{s,\ell})$, match the teacher's outputs $(\mathbf{P}^{t,g}, \mathbf{P}^{t,\ell}, C^{t,g}, C^{t,\ell})$. This is achieved by optimizing S with a specialized distillation loss $\mathcal{L}_{\text{total}}$, detailed in Section III-D.

B. Offline Teacher Caching

To enable training on a single workstation, we implement a two-stage offline caching pipeline (Fig. 1). By pre-computing teacher predictions, we decouple the heavy inference cost from the student training loop, transforming the distillation task into an accessible supervised learning problem that establishes a reproducible training recipe for labs with limited compute.

1) *Data Unification and Pre-processing*: Raw datasets are processed with a manifest generation module that performs two tasks: metadata standardization and image processing. This module processes the source images into the expected format and generates a complete *Image Manifest*.

This manifest logs normalized metadata for every processed frame, specifically: the *dataset ID*, *scene ID*, *sample ID*, *image dimensions*, and *absolute paths*. The *scene ID* groups all N views of a sequence, enabling retrieval of geometrically consistent batches. The processed image corpus and the unified manifest serve as shared input components for both offline cache generation and online student training.

2) *Cache Generation and Export*: For each sample in the manifest, the pipeline loads the corresponding images and passes them as a joint batch to the teacher. This single forward pass generates the full set of four supervision maps $(\mathbf{P}^{t,g}, \mathbf{P}^{t,\ell}, C^{t,g}, C^{t,\ell})$ as formally defined in Sec. III-A.

These raw, high-precision outputs then undergo processing to optimize storage efficiency and I/O throughput:

- 1) *Resolution alignment*. The raw teacher outputs are down-sampled to a target resolution of 224×518 . This resolution is deliberately chosen to be divisible by the 14×14 patch size of the student's DUNE encoder [74]. Pre-aligning resolutions eliminates the need for on-the-fly resizing, preventing aliasing artifacts and removing interpolation overhead that can overload CPUs during the training loop.
- 2) *Supervision filtering*. We filter predictions using the teacher's own uncertainty. We apply a confidence threshold $\tau = 0.3$ to the local confidence map $C^{t,\ell}$, following empirical guidelines for pointmap regression models [1], [14], to generate a binary *validity mask* \mathcal{M} . Pixels where $c_{ij}^{t,\ell} < \tau$ are explicitly masked and ignored by the loss function (Sec. III-D), preventing the student from learning teacher errors and decreasing computation overhead during training.
- 3) *Compression*. Given the $7\times$ storage expansion from raw data to cache, we apply aggressive compression. Continuous maps (\mathbf{P}, C) are quantized from `float32` to `float16`, while the sparse validity masks \mathcal{M} are compressed via Run-Length Encoding (RLE). This reduces the data expansion from $7\times$ to $4\times$, ensuring that data throughput remains high enough to saturate the GPU and minimize idle time during the student training loop.
- 4) *Serialization and stacking*. The processed data for all N views are aggregated. Instead of saving individual files, we stack the N maps along the batch dimension and

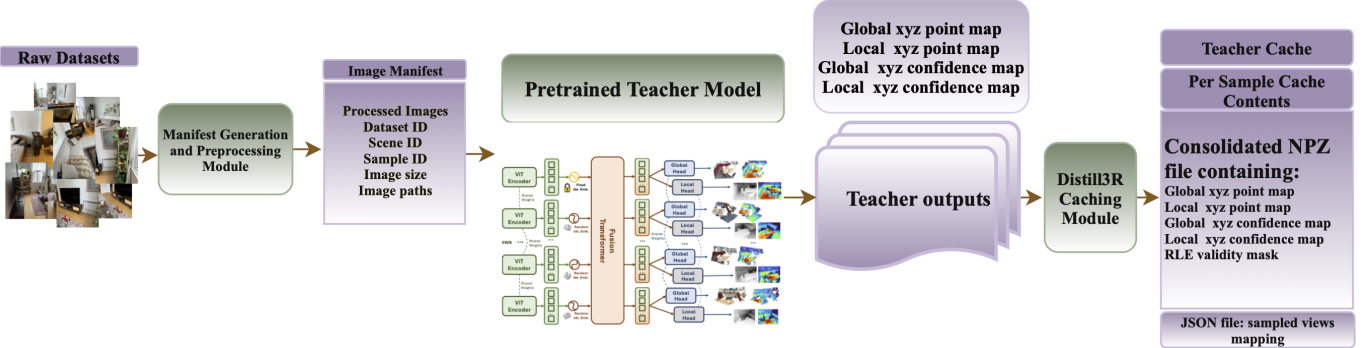


Fig. 1: An overview of the offline teacher caching pipeline. We decouple training by pre-computing teacher supervision. A Manifest Generation module indexes raw data, which is processed by Fast3R in fixed-size samples. The caching module compresses predictions (float16) and masks (RLE) into a compressed static cache used by the student and teacher dataset modules for training.

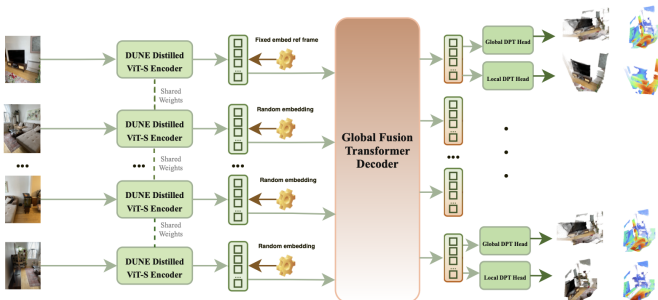


Fig. 2: Student Architecture. DUNE ViT-S encoder followed by a 6L/384d Global Fusion Transformer and DPT heads.

save them into a single consolidated archive. This consolidation is a necessary I/O optimization: it reduces file system interactions by orders of magnitude, preventing file-handle constraints and ensuring data loading keeps pace with the GPU.

C. Student Model Architecture

We design the student S to mirror the teacher's global reasoning capabilities while fitting within consumer hardware constraints and significantly reducing the parameter count. As shown in Fig. 2, we retain the meta-architecture of the teacher, but replace heavy components with lightweight alternatives.

Encoder. Instead of the teacher's heavy CroCo [83] backbone, we employ *DUNE ViT-S* [74] with weights shared across all N views. DUNE is selected for its robust 3D-aware feature space and small parameter count that outperforms larger baselines.

Embeddings. Input images are divided into non-overlapping 14x14 patches. Following Fast3R, learned positional embeddings are added to these patch tokens to encode spatial information. The first view is set as the reference frame by default. We add a fixed embedding to the reference frame because it represents the origin in the global coordinate frame. Randomized view ID embeddings are used for subsequent

views, enabling the model to distinguish between different viewpoints while providing implicit data augmentation through randomized assignment at each forward pass.

Global fusion decoder and dense prediction heads. We retain the global self-attention mechanism to resolve scale and alignment implicitly across views but we significantly reduce the depth and width relative to the teacher. This fused representation is then decoded by two lightweight DPT heads [84] to predict global ($\mathbf{P}^{s,g}$) and local ($\mathbf{P}^{s,\ell}$) coordinates along with their confidences.

D. Distillation loss function

Our total distillation loss, $\mathcal{L}_{\text{total}}$, is designed to transfer both geometric accuracy and implicitly learned uncertainty from the teacher to the student. It is a weighted sum of three loss components: a loss for the global 3D point map, a loss for the local 3D point map, and a loss for the local and global confidence maps.

All loss components are computed only on the set of valid pixels \mathcal{M} , as defined by the validity mask (Section III-B). Let $|\mathcal{M}|$ be the total number of valid pixels in a batch. The total loss is defined as:

$$\mathcal{L}_{\text{total}} = \mathcal{L}_{\text{geom_total}} + \gamma \mathcal{L}_{\text{conf}}, \quad (1)$$

where α_g , α_ℓ , and γ are hyperparameters balancing the loss terms. Based on our experiments, the gradient magnitudes for the confidence loss require down-weighting and the global geometry loss requires an increased weight: $\alpha_g = 2.0$, $\alpha_\ell = 1.0$, and $\gamma = 0.001$.

1) *Confidence-aware geometric loss:* The primary objective is to regress the teacher's dense geometry. We define the geometric loss for both global (g) and local (ℓ) heads as a weighted MSE:

$$\mathcal{L}_{\text{geo}} = \frac{1}{|\mathcal{M}|} \sum_{k \in \mathcal{I}} \sum_{(i,j) \in \mathcal{M}_k} w_{k,ij}^m \|\mathbf{p}_{k,ij}^{s,m} - \mathbf{p}_{k,ij}^{t,m}\|_2^2, \quad (2)$$

where $m \in \{g, \ell\}$ denotes the global or local coordinate map being regressed and $w_{k,ij}^m$ denotes the cached teacher confi-

dence. The total geometric contribution to the final objective is defined as:

$$\mathcal{L}_{\text{geom_total}} = \alpha_g \mathcal{L}_g + \alpha_\ell \mathcal{L}_\ell. \quad (3)$$

A primary contribution of this loss is the design of the weighting term $w_{k,ij}^m$. We explicitly derive this weight from the teacher's cached confidence C^t , rather than the student's predicted confidence C^s . In standard uncertainty-aware regression, models often learn to predict low confidence ($C^s \rightarrow 0$) to attenuate the loss in difficult regions [1], [85], leading to degenerate solutions early in training. By setting the loss weighting to the fixed calibrated teacher confidence, we prevent this collapse [78], [85], providing a stable optimization landscape that allows for successful convergence even within the shorter training cycles necessitated by resource-constrained environments. The teacher's confidence acts as a stable signal, forcing the student to prioritize high-certainty geometric areas while down-weighting uncertain regions.

Scale-invariant normalization. To enforce geometric learning, distinct normalization strategies are used. For the global loss \mathcal{L}_g , we normalize all views using a shared scale factor s computed across the entire batch:

$$\tilde{\mathbf{p}}_{k,ij}^g = \frac{\mathbf{p}_{k,ij}^g}{s}, \quad s = \frac{1}{|\mathcal{M}|} \sum_{k \in \mathcal{I}} \sum_{(i,j) \in \mathcal{M}_k} \|\mathbf{p}_{k,ij}^g\|_2. \quad (4)$$

This shared scalar enforces a consistent global coordinate frame. Conversely, for the local loss \mathcal{L}_ℓ , each view is normalized independently by its own view-specific scale factor s_k :

$$\tilde{\mathbf{p}}_{k,ij}^\ell = \frac{\mathbf{p}_{k,ij}^\ell}{s_k}, \quad s_k = \frac{1}{|\mathcal{M}_k|} \sum_{(i,j) \in \mathcal{M}_k} \|\mathbf{p}_{k,ij}^\ell\|_2. \quad (5)$$

This ensures the model generalizes to arbitrary view combinations rather than overfitting to the absolute scale of training scenes.

2) *Confidence distillation loss:* We directly distill the teacher's confidence maps. This teaches the student to reproduce the teacher's uncertainty calibration, which is important for geometric reliability and for downstream applications that use this confidence signal [85]. The student's confidence outputs ($C^{s,g}, C^{s,\ell}$) are supervised using a mean L1 loss against the cached teacher confidences ($C^{t,g}, C^{t,\ell}$) over the valid pixel mask \mathcal{M} :

$$\mathcal{L}_{\text{conf}} = \frac{1}{2|\mathcal{M}|} \sum_{k \in \mathcal{I}} \sum_{(i,j) \in \mathcal{M}_k} (|c_{k,ij}^{s,g} - c_{k,ij}^{t,g}| + |c_{k,ij}^{s,\ell} - c_{k,ij}^{t,\ell}|). \quad (6)$$

This loss, combined with geometric losses, encourages the student model to learn a complete representation of the 3D scene.

IV. EXPERIMENTS

Compute setup. All models are trained on a single workstation equipped with two NVIDIA RTX 6000 Ada (48 GB) GPUs. The full training pipeline is also verified to run on a

single GPU without modification. Unless otherwise stated, all experiments and evaluations are conducted using a single RTX 6000 Ada GPU.

Datasets. The training set is constructed from six established datasets following Fast3R: CO3D-v2 [61], ScanNet++ [67], Habitat [86], MegaDepth [65], BlendedMVS [66], and ARKitScenes [27]. This mix ensures that the student sees a wide distribution of scene types, scene scales, lighting conditions, and sensor characteristics, ranging from object-centric captures, indoor navigation, to large-scale outdoor scenes.

Dynamic sub-sampling strategy. Training on all available frames is computationally redundant due to the high overlap between frames which makes frame to frame variation indistinguishable in most scenes. To maximize geometric variance while minimizing dataset size, a dynamic sub-sampling strategy is used. The sampling stride is adjusted based on scene type, overlap, and number of images. For example, in object-centric data (CO3D [61]), a wide baseline dependent on the number of images is used to encourage global understanding; for navigation datasets (Habitat [86], ScanNet++ [67]), the stride is increased proportional to trajectory length to ensure sufficient overlap for feature matching; for large outdoor scenes (MegaDepth [65]), the stride is increased based on scene size assuming significant overlap and redundant information. We sample $N = 20$ contiguous frames following [9]. This strict temporal locality preserves the consistency required for the student's global fusion mechanism to learn cross-view correspondences. [82]. This process distills the multi-terabyte corpus down to a dense training set of approximately 450k images (150 GB).

Student Architecture. Our 72 M-parameter student model consists of three key components:

- 1) *Image Encoder.* DUNE ViT-Small (21M) initialized with DUNE pretrained weights. It operates on 14×14 patches with weights shared across all N views.
- 2) *Fusion Transformer.* We replace the teacher's heavy decoder with a compressed transformer (6 layers, 6 heads, 384 embedding dim) initialized from scratch. It uses cross view self-attention to fuse features across the view sequence.
- 3) *Pointmap Heads.* Two lightweight DPT heads regress dense global/local coordinates and confidence maps.

Training Pipeline. To make training possible on a single workstation, the training loop assumes that the cache has already been generated. As a result, the training process is similar to standard supervised training. The cache and manifest represent the dataset and are processed using the student dataset module and teacher dataset module as depicted in Fig. 3. The student dataset module retrieves image batches and the associated teacher-sampled paths for those images from the manifest. In parallel, the teacher dataset module fetches pre-computed supervision signals (geometry and confidence) directly from the consolidated cache corresponding to paths processed by the student dataset module for that batch. The stacking step in cache processing ensures that we do not reach file handle limits and overload the CPU cores on a single

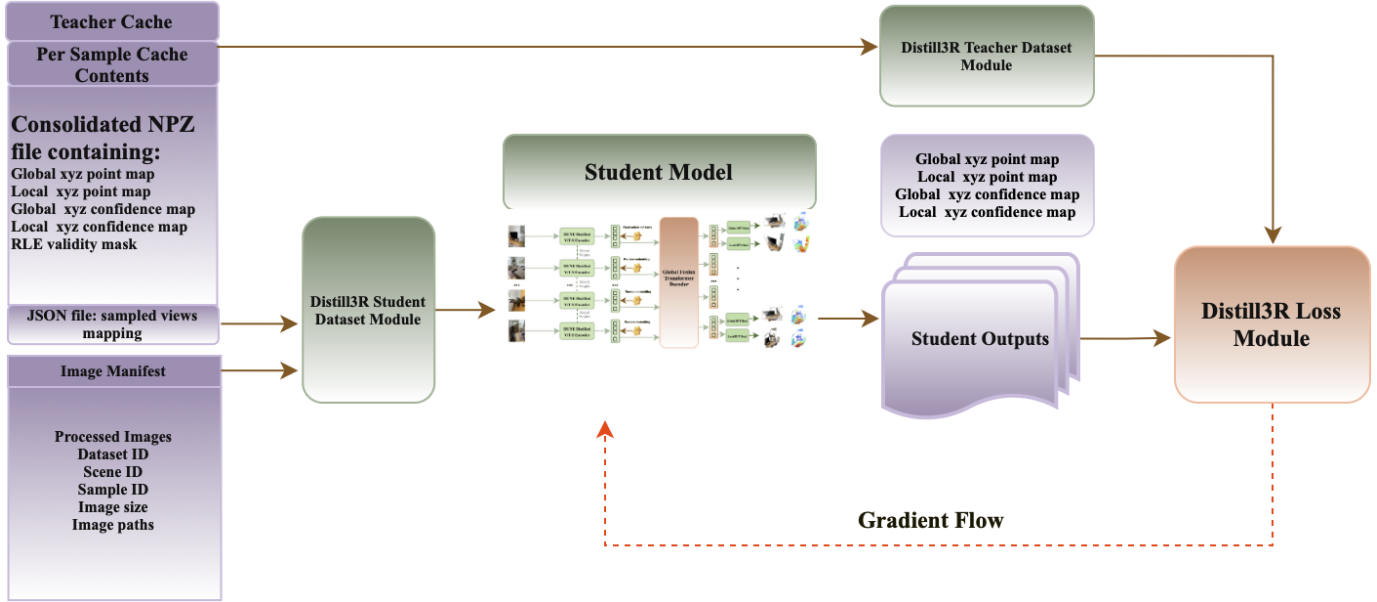


Fig. 3: An overview of the Distill3R training loop. (1) The Distill3R Student Dataset Module loads a batch of N images (from the Image Manifest) and the corresponding N pre-computed supervision signals (from the Teacher Cache). (2) The Student Model processes the images and generates its own 3D point maps and confidence maps. (3) The Distill3R Loss Module compares the Student Outputs against the cached Teacher Outputs to compute $\mathcal{L}_{\text{total}}$. (4) The resulting Gradient Flow (red dotted line) updates only the Student Model’s parameters.

workstation by aggregating all the supervision signals for each sample into single files. The cache generation is completed on a single NVIDIA RTX 6000 Ada and takes 11.3 hours.

Training Hyperparameters. Training utilizes the AdamW optimizer [87] with a weight decay of 0.01. We employ a cosine annealing schedule [88] with linear warmup for the first 3,500 steps, peaking at 1×10^{-4} before decaying to 5×10^{-5} . To maximize throughput, the model exploits bf16 mixed-precision [89] and FlashAttention [90], [91], enabling scaling to $N = 20$ views without memory exhaustion. All experiments are conducted on a single workstation with 2× NVIDIA RTX 6000 Ada (48 GB) GPUs for a total of 60 epochs over 2.875 days using a resolution of 224×518 . Using a per-GPU batch size of 4 with 2 gradient accumulation steps yields an effective batch size of 16.

A. Inference Efficiency

The motivation for Distill3R is to retain the reconstruction capabilities of large feed-forward models while drastically reducing computational overhead. We measure inference latency and peak GPU memory usage on a single NVIDIA RTX 6000 Ada Generation GPU (48 GB).

We adopt a sliding-window protocol relevant to real-time applications, scaling the number of input views $N \in \{12, 32, 64, 96, 128\}$ at a fixed resolution of 378×518 . for all models except Fast3R. Fast3R uses a fixed resolution of 384×512 to match CroCo patch size. We measure the wall-clock time required to process a single batch and track the peak VRAM usage during the forward pass. To ensure a fair

comparison, we only test single pass feed-forward models that utilize global attention because models like DUST3R that require post-processing for alignment are notably slower and more memory intensive [9]. We remove the maximum parallel views restriction for the dense predictions heads as well as chunking mechanisms on all models to ensure fair comparison by processing all input frames at once.

Results in Table I show that our student model is nearly $5 \times$ faster than the teacher model at $N = 128$ views. This divergence grows as the number of views increases. The difference in inference speed is more pronounced with VGTT where Distill3R is nearly $6 \times$ faster by $N = 64$ views.

B. 3D Reconstruction

We evaluate the geometric reconstruction quality of our distilled student model on unseen scene-level (7-Scenes [92]) and object-level (DTU [93]) benchmarks. To isolate the student’s learned geometric reasoning from rotational bottlenecks in global alignment, we perform a per-view evaluation. Fast3R also evaluates reconstruction using the local head while using ICP for global alignment [9].

As reported in Table II, the student model exhibits a characterized trade-off between absolute precision and metric grounding. While the teacher maintains higher fine-grained regression accuracy, our 72 M student demonstrates a significantly superior adherence to absolute metric scale across both indoor and extreme out-of-distribution (OOD) object-centric scenes.

TABLE I: System efficiency comparison on RTX 6000 Ada. Performance metrics for varying view counts (N). Time is measured in seconds (s) and Peak Memory in GB. OOM denotes Out Of Memory. All methods except Fast3R are evaluated at 378×518 resolution; Fast3R uses 384×512 . Bold and underline indicate the best and second-best results, respectively.

Method	$N = 12$		$N = 32$		$N = 64$		$N = 96$		$N = 128$	
	Time (s)	Mem (GB)	Time (s)	Mem (GB)	Time (s)	Mem (GB)	Time (s)	Mem (GB)	Time (s)	Mem (GB)
Fast3R (Teacher) [9]	0.32	6.86	1.14	12.11	3.26	21.11	6.35	32.36	10.11	44.36
VGGT [10]	0.59	15.28	2.28	33.98	6.40	38.41	OOM	OOM	OOM	OOM
Distill3R (Ours)	0.13	4.05	0.41	9.97	1.02	21.80	1.78	28.69	2.69	31.90

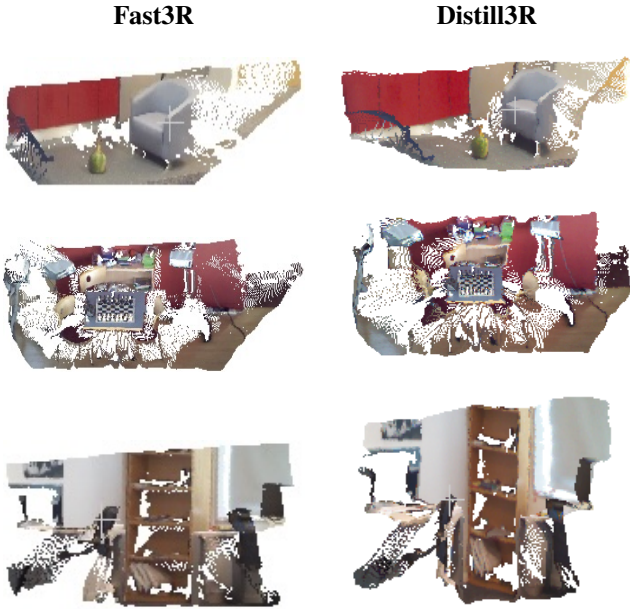


Fig. 4: **Qualitative comparison on 7-Scenes (OOD).** Side-by-side reconstructions showing that Distill3R (right) preserves the global topology of the teacher (left).

On the 7-Scenes benchmark, the student achieves an average scale factor of 1.62, closely approaching true metric scale (1.0). In contrast, the 650 M teacher exhibits an average scale factor of 3.54, requiring heavy post-hoc scaling to match real-world dimensions. These results suggest that the distillation process regularizes the student toward a more grounded metric prior. For robotics applications, such as navigation initialization and reactive mapping, this metric stability is often more valuable than high-frequency textural precision. While quantitative metrics saturate early, qualitative analysis (Fig. 5) reveals significant improvements in structural coherence and surface smoothness as training progresses to 60 epochs. As observed in Table III, the primary quantitative shift during extended training is a slight degradation in the completeness metric, while accuracy and metric scale continue to improve.

V. ABLATIONS

A. Encoder

The first stage is a 2D feature encoder that extracts patch-level embeddings from each input image I_k . We selected

TABLE II: Quantitative Reconstruction Results. Per-view evaluation. Metrics are Median Distance (Acc/Comp) scaled by $100 \times$. Scale factor measures adherence to true metric scale (1.0 is perfect). Bold indicates the best results. Note: 7-Scenes ground truth is in meters, while DTU is in millimeters, accounting for the magnitude difference in scale factors.

Method	7-Scenes (OOD)			DTU (OOD)		
	Acc \downarrow	Comp \downarrow	Scale \downarrow	Acc \downarrow	Comp \downarrow	Scale \downarrow
Fast3R (Teacher) [9]	2.45	2.97	3.54	0.31	0.41	942.49
Distill3R (Ours)	8.76	8.88	1.62	1.16	1.77	394.59

DUNE ViT-S [74] (21 M parameters) as our backbone. Preliminary ablations showed that DINoV3 ViT-S [18] yielded significantly poorer 3D reconstruction quality. While CroCo-B [11] is a strong baseline, the lack of a publicly available ViT-Small variant would necessitate complex architectural modifications and bespoke weight-copying to fit our student’s $d = 384$ design. DUNE’s heterogeneous co-distillation acts as a form of knowledge synthesis, providing a holistic scene representation that is better suited for dense 3D regression than single-modality teachers [74].

B. Loss Terms and Training Without Distillation

To validate our distillation objective, we ablated the specific components that leverage teacher uncertainty. These data show that removing these terms degrades the quality of the reconstruction.

Furthermore, to validate the distillation pipeline, we simulate training from scratch by removing the direct confidence supervision and replacing the teacher confidence weighting on the geometric loss with the student’s own confidence. This configuration removes the relational knowledge inherent in distillation, mimicking the standard objective used in models like Fast3R. By treating the teacher’s output point maps as pseudo-ground truth, we avoid the computational cost of global Structure-from-Motion (SfM) being used on our entire training dataset while demonstrating the necessity of distillation. This is supported by the fact that the teacher’s point maps are nearly indistinguishable from traditional SfM results in terms of structural consistency. As shown in Table III, the absence of distillation signals results in a 9.6% reduction in accuracy and a substantial 35.7% degradation in completion quality.

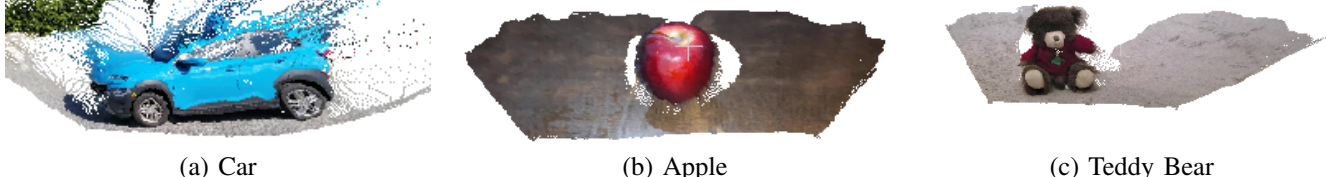


Fig. 5: Object reconstruction (CO3D-v2). Qualitative results for the Distill3R student on object-centric scenes.

TABLE III: Loss Term Ablation. Evaluated on DTU (OOD). These data show that geometric coordinate transfer alone (Labels-Only) is insufficient without teacher uncertainty signals. Bold and underline indicate the best and second-best results, respectively.

Configuration	Acc \downarrow	Comp \downarrow	Scale \downarrow
Labels-Only (No Weighting/Conf)	<u>1.37</u>	2.09	<u>409.05</u>
w/o Weighting $w_{k,ij}$	1.42	<u>1.88</u>	467.85
Distill3R (Full)	1.25	1.54	380.30

C. Discussion: A Roadmap for Efficient 3D Vision

Distill3R serves as a foundational entry point for democratized research into 3D foundation models. By providing a pipeline that can be trained on a single workstation, we lay the groundwork for future improvements in neural reconstruction.

The Pose Estimation Challenge. A primary structural limitation of the current Distill3R iteration is rotational drift in global pose estimation. The student achieves accurate translation in the global reference frame but fails to capture the required rotation to properly align views. Because the Fast3R teacher relies on ICP-based alignment to ground-truth poses during its own training, the student receives geometry that is already anchored to a reference frame without explicitly learning the rotation parameters. Using ground-truth poses combined with procedural alignment at train time would impose a significant bottleneck on dataset construction and cache generation, reducing the accessibility of the pipeline for the research community. Addressing this limitation by directly supervising camera parameters would require a substantially different training formulation and supervision signal, shifting the focus from geometry distillation toward explicit pose regression. In this context, permutation-equivariant models such as π^3 [24] represent a promising direction for future work, as they are designed to infer camera parameters without reliance on a fixed reference frame. Integrating such models into the Distill3R pipeline would enable end-to-end pose supervision, but would also entail a non-trivial expansion of the training pipeline and evaluation scope beyond the goals of the current work.

Enhancing Robustness and Metrics. To further bridge the quantitative gap identified in our benchmarks, we identify several promising directions:

- *Data Augmentation:* Implementing aspect-ratio and scale-

invariant augmentations accompanied by a matching logic in the teacher cache could improve robustness to varying sensor characteristics.

- *Geometric Priors:* Integrating a planar loss (Manhattan-world prior) could significantly improve the metrics on indoor benchmarks like 7-Scenes where warping is present.
- *Functional Scaling:* For robotics-specific applications where raw RMSE is secondary to navigation utility, researchers may explore even more aggressive compression of the fusion transformer to target ultra-low-power edge devices.

Specialized Knowledge Synthesis. The Distill3R pipeline provides a template for domain-specific specialization. By decoupling teacher inference, researchers can efficiently train compact student models on proprietary or niche datasets such as medical imaging or specific industrial environments, where a general-purpose foundation model may be too computationally expensive to deploy. This enables the creation of highly specialized, low-latency models tailored for specific sub-tasks without requiring the massive infrastructure used for initial foundation model training.

VI. CONCLUSION

In this work, we introduced Distill3R, a novel distillation framework designed to close the gap between heavyweight 3D foundation models and resource-constrained research and deployment environments. We demonstrate that the structural intelligence of 650 M-parameter models can be distilled into a student an order of magnitude smaller, achieving significantly superior adherence to absolute metric scale despite a drop in fine-grained precision. By reducing the training infrastructure requirements to a single workstation and providing a 5 \times speedup at inference time, we have laid the groundwork for future iterations to address the current global pose estimation bottlenecks by providing a modular pipeline that can integrate next-generation permutation-equivariant teachers. Distill3R serves as a proof-of-concept that high-capacity 3D vision can be democratized. By shifting the focus from over-parameterization to efficient distillation and knowledge synthesis, the community can accelerate the deployment of these models onto mobile robots and embedded systems. Additionally, Distill3R provides an accessible research baseline that enables laboratories without large-scale compute to train and specialize 3D models on their own domain-specific data at minimal cost.

REFERENCES

- [1] S. Wang, V. Leroy, Y. Cabon, B. Chidlovskii, and J. Revaud, “DUSt3R: Geometric 3D vision made easy,” in *Proceedings of the IEEE/CVF Conference on Computer Vision and Pattern Recognition*, 2024, pp. 20 697–20 709.
- [2] H. Cui, X. Gao, S. Shen, and Z. Hu, “HSFM: Hybrid structure-from-motion,” in *Proceedings of the IEEE/CVF Conference on Computer Vision and Pattern Recognition*, 2017, pp. 1212–1221.
- [3] X. Wei, Y. Zhang, Z. Li, Y. Fu, and X. Xue, “DeepSFM: Structure from motion via deep bundle adjustment,” in *Proceedings of the European Conference on Computer Vision*. Springer, 2020, pp. 230–247.
- [4] J. L. Schönberger and J.-M. Frahm, “Structure-from-motion revisited,” in *Proceedings of the IEEE/CVF Conference on Computer Vision and Pattern Recognition*, 2016, pp. 4104–4113.
- [5] S. Agarwal, N. Snavely, I. Simon, S. M. Seitz, and R. Szeliski, “Building Rome in a day,” in *Proceedings of the IEEE/CVF International Conference on Computer Vision*, 2009, pp. 72–79.
- [6] R. Hartley and A. Zisserman, *Multiple View Geometry in Computer Vision*, 1st ed. Cambridge University Press, 2000.
- [7] N. Snavely, S. M. Seitz, and R. Szeliski, “Photo tourism: Exploring photo collections in 3D,” in *Proceedings of ACM SIGGRAPH*, 2006, pp. 835–846.
- [8] O. Özyessil, V. Voroninski, R. Basri, and A. Singer, “A survey of structure from motion,” *Acta Numerica*, vol. 26, pp. 305–364, 2017.
- [9] J. Yang *et al.*, “Fast3R: Towards 3D reconstruction of 1000+ images in one forward pass,” in *Proceedings of the IEEE/CVF Conference on Computer Vision and Pattern Recognition*, 2025, pp. 21 924–21 935.
- [10] J. Wang, M. W. Chen, N. Karaev, C. Rupprecht, and D. Novotny, “VGFT: Visual geometry grounded transformer,” in *Proceedings of the IEEE/CVF Conference on Computer Vision and Pattern Recognition*, 2025, pp. 5294–5306.
- [11] V. Leroy, Y. Cabon, and J. Revaud, “Grounding image matching in 3d with mast3r,” in *Proceedings of the European Conference on Computer Vision*, 2024, pp. 71–91.
- [12] S. Zhang *et al.*, “FLARE: Feed-forward geometry, appearance and camera estimation from uncalibrated sparse views,” in *Proceedings of the IEEE/CVF Conference on Computer Vision and Pattern Recognition*, 2025, pp. 21 936–91 947.
- [13] J. Zhang *et al.*, “MonST3R: A simple approach for estimating geometry in the presence of motion,” in *Proceedings of the IEEE/CVF Conference on Computer Vision and Pattern Recognition*, 2025, pp. 6273–6282.
- [14] Z. Tang *et al.*, “MV-DUSt3R+: Single-stage scene reconstruction from sparse views in 2 seconds,” in *Proceedings of the IEEE/CVF Conference on Computer Vision and Pattern Recognition*, 2024, pp. 5283–5293.
- [15] B. Duisterhof *et al.*, “MASt3R-SfM: A fully-integrated solution for unconstrained structure-from-motion,” in *Proceedings of the International Conference on 3D Vision*, 2024.
- [16] T. B. Brown *et al.*, “Language models are few-shot learners,” *arXiv preprint arXiv:2005.14165*, 2020.
- [17] A. Dosovitskiy *et al.*, “An image is worth 16x16 words: Transformers for image recognition at scale,” in *Proceedings of the International Conference on Learning Representations*, 2021.
- [18] O. Siméoni *et al.*, “DINOv3: Self-supervised learning for vision at unprecedented scale,” *arXiv preprint arXiv:2508.10104*, 2025.
- [19] J. Achiam *et al.*, “GPT-4 technical report,” *arXiv preprint arXiv:2303.08774*, 2023.
- [20] A. Radford *et al.*, “Learning transferable visual models from natural language supervision,” in *Proceedings of the International Conference on Machine Learning*, 2021, pp. 8748–8763.
- [21] J. Kaplan *et al.*, “Scaling laws for neural language models,” *arXiv preprint arXiv:2001.08361*, 2020.
- [22] J. Hoffmann *et al.*, “Training compute-optimal large language models,” *arXiv preprint arXiv:2203.15556*, 2022.
- [23] W. Peebles and S. Xie, “Scalable diffusion models with transformers,” in *Proceedings of the IEEE/CVF International Conference on Computer Vision*, 2023, pp. 4195–4205.
- [24] Y. Wang *et al.*, “ π^3 : Permutation-equivariant visual geometry learning,” *arXiv preprint arXiv:2507.13347*, 2025.
- [25] K. Wu *et al.*, “TinyViT: Fast pretraining distillation for small vision transformers,” in *Proceedings of the European Conference on Computer Vision*, 2022.
- [26] H. Xia, Y. Fu, S. Liu, and X. Wang, “RGBD objects in the wild: Scaling real-world 3D object learning from RGB-D videos,” in *Proceedings of the IEEE/CVF Conference on Computer Vision and Pattern Recognition*, 2024, pp. 22 378–22 389.
- [27] G. Baruch *et al.*, “ARKitScenes: A diverse real-world dataset for 3D indoor scene understanding using mobile RGB-D data,” in *Advances in Neural Information Processing Systems*, 2021.
- [28] X. Pan *et al.*, “Aria digital twin: A new benchmark dataset for egocentric 3D machine perception,” in *Proceedings of the IEEE/CVF International Conference on Computer Vision*, 2023, pp. 20 133–20 143.
- [29] A. Szot *et al.*, “Habitat 2.0: Training home assistants to rearrange their habitat,” in *Advances in Neural Information Processing Systems*, 2021.
- [30] X. Sun *et al.*, “AVGGT: Rethinking global attention for accelerating VGGT,” *arXiv preprint arXiv:2512.02541*, 2025.
- [31] C.-S. B. Wang, C. Schmidt, J. Piekenbrinck, and B. Leibe, “Faster VGGT with block-sparse global attention,” *arXiv preprint arXiv:2509.07120*, 2025.
- [32] C.-S. B. Wang, C. Schmidt, D. Noytyn, and C. Rupprecht, “FastVGGT: Training-free acceleration of visual geometry transformer,” *arXiv preprint arXiv:2509.02560*, 2025.
- [33] W. Feng *et al.*, “Quantized visual geometry grounded transformer,” *arXiv preprint arXiv:2509.21302*, 2025.
- [34] G. E. Hinton, O. Vinyals, and J. Dean, “Distilling the knowledge in a neural network,” *arXiv preprint arXiv:1503.02531*, 2015.
- [35] J. Gou, B. Yu, S. J. Maybank, and D. Tao, “Knowledge distillation: A survey,” *International Journal of Computer Vision*, vol. 129, no. 6, pp. 1789–1819, 2021.
- [36] H. Touvron *et al.*, “Training data-efficient image transformers & distillation through attention,” in *Proceedings of the International Conference on Machine Learning*, 2021, pp. 10 347–10 357.
- [37] A. Hornung, K. M. Wurm, M. Bennewitz, C. Stachniss, and W. Burgard, “Octomap: An efficient probabilistic 3d mapping framework based on octrees,” *Autonomous Robots*, vol. 34, pp. 189–206, 2013.
- [38] A. J. Davison, I. D. Reid, N. D. Molton, and O. Stasse, “Monoslam: Real-time single camera slam,” *IEEE Transactions on Pattern Analysis and Machine Intelligence*, vol. 29, no. 6, pp. 1052–1067, 2007.
- [39] Z. Teed and J. Deng, “DROID-SLAM: Deep visual SLAM for monocular, stereo, and RGB-D cameras,” in *Advances in Neural Information Processing Systems*, vol. 34, 2021, pp. 16 558–16 569.
- [40] T. Qin, P. Li, and S. Shen, “Vins-mono: A robust and versatile monocular visual-inertial state estimator,” *IEEE Transactions on Robotics*, vol. 34, no. 4, pp. 1004–1020, 2018.
- [41] R. Hartley and A. Zisserman, *Multiple View Geometry in Computer Vision*, 2nd ed. Cambridge University Press, 2004.
- [42] D. DeTone, T. Malisiewicz, and A. Rabinovich, “SuperPoint: Self-supervised interest point detection and description,” in *Proceedings of the IEEE/CVF Conference on Computer Vision and Pattern Recognition Workshops*, 2018, pp. 224–236.
- [43] M. Dusmanu *et al.*, “D2-Net: A trainable CNN for joint description and detection of local features,” in *Proceedings of the IEEE/CVF Conference on Computer Vision and Pattern Recognition*, 2019, pp. 8092–8101.
- [44] X. Zhao *et al.*, “ALIKED: A lighter keypoint and descriptor extraction network via deformable transformation,” *IEEE Trans. Instrum. Meas.*, vol. 72, pp. 1–16, 2023.
- [45] K. M. Yi, E. Trulls, V. Lepetit, and P. Fua, “LIFT: Learned invariant feature transform,” in *Proceedings of the European Conference on Computer Vision*, 2016, pp. 467–483.
- [46] D. G. Lowe, “Distinctive image features from scale-invariant keypoints,” *International Journal of Computer Vision*, vol. 60, no. 2, pp. 91–110, 2004.
- [47] P.-E. Sarlin, D. DeTone, T. Malisiewicz, and A. Rabinovich, “SuperGlue: Learning feature matching with graph neural networks,” in *Proceedings of the IEEE/CVF Conference on Computer Vision and Pattern Recognition*, 2020, pp. 4938–4947.
- [48] J. Sun, Z. Shen, Y. Wang, H. Bao, and X. Zhou, “LoFTR: Detector-free local feature matching with transformers,” in *Proceedings of the IEEE/CVF Conference on Computer Vision and Pattern Recognition*, 2021, pp. 8922–8931.
- [49] J. Edstedt, Q. Sun, G. Bökman, M. Wadenbäck, and M. Felsberg, “RoMa: Robust dense feature matching,” in *Proceedings of the IEEE/CVF Conference on Computer Vision and Pattern Recognition*, 2024, pp. 19 790–19 800.

- [50] P. Lindenberger, P.-E. Sarlin, and M. Pollefeys, “LightGlue: Local feature matching at light speed,” in *Proceedings of the IEEE/CVF International Conference on Computer Vision*, 2023, pp. 17 627–17 638.
- [51] Y. Yao, Z. Luo, S. Li, T. Fang, and L. Quan, “MVSNet: Depth inference for unstructured multi-view stereo,” in *Proceedings of the European Conference on Computer Vision*, 2018.
- [52] X. Gu *et al.*, “Cascade cost volume for high-resolution multi-view stereo and stereo matching,” in *Proceedings of the IEEE/CVF Conference on Computer Vision and Pattern Recognition*, 2020, pp. 2495–2504.
- [53] B. Cheng, I. Misra, A. G. Schwing, A. Kirillov, and R. Girdhar, “Masked-attention mask transformer for universal image segmentation,” in *Proceedings of the IEEE/CVF Conference on Computer Vision and Pattern Recognition*, 2022, pp. 1290–1299.
- [54] C. Wu, “Towards linear-time incremental structure from motion,” in *Proceedings of the International Conference on 3D Vision*. IEEE, 2013, pp. 127–134.
- [55] J. Edst  d, I. Athanasiadis, M. Wadenb  ck, and M. Felsberg, “DKM: Dense kernelized feature matching for geometry estimation,” in *Proceedings of the IEEE/CVF Conference on Computer Vision and Pattern Recognition*, 2023, pp. 17 765–17 775.
- [56] M. Tyszkiewicz, P. Fua, and E. Trulls, “DISK: Learning local features with policy gradient,” in *Advances in Neural Information Processing Systems*, vol. 33, 2020, pp. 14 254–14 265.
- [57] M. Caron *et al.*, “Emerging properties in self-supervised vision transformers,” in *Proceedings of the IEEE/CVF International Conference on Computer Vision*, 2021, pp. 9650–9660.
- [58] J. Wang, N. Karaev, C. Rupprecht, and D. Novotny, “VGGsFm: Visual geometry grounded deep structure from motion,” in *Proceedings of the IEEE/CVF Conference on Computer Vision and Pattern Recognition*, 2024, pp. 21 686–21 697.
- [59] C. Tang and P. Tan, “BA-Net: Dense bundle adjustment network,” *arXiv preprint arXiv:1806.04807*, 2018.
- [60] Z. Teed and J. Deng, “DeepV2D: Video to depth with differentiable structure from motion,” *arXiv preprint arXiv:1812.04605*, 2018.
- [61] J. Reizenstein *et al.*, “Common objects in 3D: Large-scale learning and evaluation of real-life 3D category reconstruction,” in *Proceedings of the IEEE/CVF International Conference on Computer Vision*, 2021, pp. 10 901–10 911.
- [62] A. Dai *et al.*, “ScanNet: Richly-annotated 3D reconstructions of indoor scenes,” in *Proceedings of the IEEE/CVF Conference on Computer Vision and Pattern Recognition*, 2017, pp. 5828–5839.
- [63] Y. Zheng, A. W. Harley, B. Shen, G. Wetzstein, and L. J. Guibas, “PointOdyssey: A large-scale synthetic dataset for long-term point tracking,” in *Proceedings of the IEEE/CVF International Conference on Computer Vision*, 2023, pp. 19 855–19 865.
- [64] M. Deitke *et al.*, “Objaverse: A universe of annotated 3D objects,” in *Proceedings of the IEEE/CVF Conference on Computer Vision and Pattern Recognition*, 2023, pp. 13 142–13 153.
- [65] Z. Li and N. Snavely, “MegaDepth: Learning single-view depth prediction from internet photos,” in *Proceedings of the IEEE/CVF Conference on Computer Vision and Pattern Recognition*, 2018, pp. 2041–2050.
- [66] Y. Yao *et al.*, “BlendedMVS: A large-scale dataset for generalized multi-view stereo networks,” in *Proceedings of the IEEE/CVF Conference on Computer Vision and Pattern Recognition*, 2020, pp. 1790–1799.
- [67] C. Yeshwanth, Y.-C. Liu, M. Nie  ner, and A. Dai, “ScanNet++: A high-fidelity dataset of 3D indoor scenes,” in *Proceedings of the IEEE/CVF International Conference on Computer Vision*, 2023, pp. 12–22.
- [68] Y. Cabon *et al.*, “MUSt3R: Multi-view network for stereo 3D reconstruction,” in *Proceedings of the IEEE/CVF Conference on Computer Vision and Pattern Recognition*, 2025.
- [69] W. Jang, P. Weinzaepfel, V. Leroy, L. Agapito, and J. Revaud, “Pow3R: Empowering unconstrained 3D reconstruction with camera and scene priors,” in *Proceedings of the IEEE/CVF Conference on Computer Vision and Pattern Recognition*, 2025.
- [70] S. Wang *et al.*, “Spann3R: Towards reliable and efficient dense pipeline for 3D reconstruction,” in *Proceedings of the International Conference on 3D Vision*, 2025.
- [71] V. Lepetit, F. Moreno-Noguer, and P. Fua, “EPnP: An accurate $o(n)$ solution to the pnp problem,” *International Journal of Computer Vision*, vol. 81, pp. 155–166, 2009.
- [72] J. Wang, C. Rupprecht, and D. Novotny, “PoseDiffusion: Solving pose estimation via diffusion-aided bundle adjustment,” in *Proceedings of the IEEE/CVF International Conference on Computer Vision*, 2023, pp. 9773–9783.
- [73] A. Kendall, M. Grimes, and R. Cipolla, “PoseNet: A convolutional network for real-time 6-DOF camera relocalization,” in *Proceedings of the IEEE/CVF International Conference on Computer Vision*, 2015, pp. 2938–2946.
- [74] M. B. Sar  yildiz *et al.*, “DUNE: Distilling a universal encoder from heterogeneous 2D and 3D teachers,” in *Proceedings of the IEEE/CVF Conference on Computer Vision and Pattern Recognition*, 2025.
- [75] Y. Wei, S. Liu, Y. Rao, W. Zhao, J. Lu, and J. Zhou, “NeRfingMVS: Guided optimization of neural radiance fields for indoor multi-view stereo,” in *Proceedings of the IEEE/CVF International Conference on Computer Vision*, 2021, pp. 5610–5619.
- [76] J. Tang *et al.*, “LGM: Large multi-view Gaussian model for high-resolution 3D content creation,” in *Proceedings of the European Conference on Computer Vision*, 2024, pp. 1–18.
- [77] L. Yang *et al.*, “Depth Anything v2,” *arXiv preprint arXiv:2406.09414*, 2024.
- [78] Z. Wu *et al.*, “ADU-Depth: Attention-based distillation with uncertainty modeling for depth estimation,” in *Advances in Neural Information Processing Systems*, 2023.
- [79] J. Song and S. J. Lee, “Knowledge distillation of multi-scale dense prediction transformer for self-supervised depth estimation,” *Sci. Rep.*, vol. 13, no. 1, p. 18939, 2023.
- [80] Y. Ding *et al.*, “KD-MVS: Knowledge distillation based self-supervised learning for multi-view stereo,” in *Proceedings of the European Conference on Computer Vision*, 2022, pp. 610–627.
- [81] A. Dutt, M. Kaur, and I. Lunawat, “Multi-view 3D reconstruction using knowledge distillation,” *Stanford CS231A Reports*, 2024.
- [82] M. Stary, J. Gaubil, A. Tewari, and V. Sitzmann, “Understanding multi-view transformers,” *arXiv preprint arXiv:2510.24907*, 2025.
- [83] P. Weinzaepfel *et al.*, “CroCo: Self-supervised pre-training for 3D vision tasks by cross-view completion,” in *Advances in Neural Information Processing Systems*, vol. 35, 2022, pp. 3502–3516.
- [84] R. Ranftl, A. Bochkovskiy, and V. Koltun, “Vision transformers for dense prediction,” in *Proceedings of the IEEE/CVF International Conference on Computer Vision*, 2021, pp. 12 179–12 188.
- [85] A. Kendall and Y. Gal, “What uncertainties do we need in bayesian deep learning for computer vision?” in *Advances in Neural Information Processing Systems*, 2017, pp. 5580–5590.
- [86] M. Savva *et al.*, “Habitat: A platform for embodied AI research,” in *Proceedings of the IEEE/CVF International Conference on Computer Vision*, 2019, pp. 9339–9347.
- [87] I. Loshchilov and F. Hutter, “Decoupled weight decay regularization,” in *Proceedings of the International Conference on Learning Representations*, 2019.
- [88] ———, “SGDR: Stochastic gradient descent with warm restarts,” in *Proceedings of the International Conference on Learning Representations*, 2017.
- [89] P. Micikevicius *et al.*, “Mixed precision training,” in *Proceedings of the International Conference on Learning Representations*, 2018.
- [90] T. Dao, D. Y. Fu, S. Ermon, A. Rudra, and C. R  , “FlashAttention: Fast and memory-efficient exact attention with IO-awareness,” in *Advances in Neural Information Processing Systems*, vol. 35, 2022, pp. 16 344–16 359.
- [91] T. Dao, “FlashAttention-2: Faster attention with better parallelism and work partitioning,” in *Advances in Neural Information Processing Systems*, vol. 36, 2023, pp. 35 204–35 219.
- [92] J. Shotton *et al.*, “Scene coordinate regression forests for camera relocalization in RGB-D images,” in *Proceedings of the IEEE/CVF Conference on Computer Vision and Pattern Recognition*, 2013, pp. 2930–2937.
- [93] H. Aan  s *et al.*, “Large-scale data for multiple-view stereopsis,” *International Journal of Computer Vision*, vol. 120, pp. 153–168, 2016.